mathematics

Article

Feature Selection Fuzzy Neural Network Super-Twisting Harmonic Control

Qi Pan [1,2], Yanli Zhou [2] and Juntao Fei [1,2,3,*]

[1] College of IoT Engineering, Hohai University, Changzhou 213022, China
[2] College of Mechanical and Electrical Engineering, Hohai University, Changzhou 213022, China
[3] Jiangsu Key Laboratory of Power Transmission and Distribution Equipment Technology, Hohai University, Changzhou 213022, China
* Correspondence: jtfei@hhu.edu.cn

Abstract: This paper provides a multi-feedback feature selection fuzzy neural network (MFFSFNN) based on super-twisting sliding mode control (STSMC), aiming at compensating for current distortion and solving the harmonic current problem in an active power filter (APF) system. A feature selection layer is added to an output feedback neural network to attach the characteristics of signal filtering to the neural network. MFFSFNN, with the designed feedback loops and hidden layer, has the advantages of signal judging, filtering, and feedback. Signal filtering can choose valuable signals to deal with lumped uncertainties, and signal feedback can expand the learning dimension to improve the approximation accuracy. The STSMC, as a compensator with adaptive gains, helps to stabilize the compensation current. An experimental study is implemented to prove the effectiveness and superiority of the proposed controller.

Keywords: active power filter; fuzzy neural network; multi-feedback feature selection super-twisting sliding mode control

MSC: 68T07; 93C40

check for updates

Citation: Pan, Q.; Zhou, Y.; Fei, J. Feature Selection Fuzzy Neural Network Super-Twisting Harmonic Control. *Mathematics* **2023**, *11*, 1495. https://doi.org/10.3390/math11061495

Academic Editors: Mostefa Mohamed-Seghir and Józef Lisowski

Received: 16 February 2023
Revised: 13 March 2023
Accepted: 16 March 2023
Published: 18 March 2023

1. Introduction

With the wide application of distributed power generation and electronic transformers, the construction of modern power grids is developing more electronics. However, because the access of electronic equipment to power grids has become more frequent nowadays, non-linear characteristics of the load are more prominent. As a result, harmonic pollution has increased compared to the past. When the harmonic current flows through the system, harmonic voltage is generated and has an adverse effect on electronic equipment. Nowadays, smart devices are widely used in grids, which are more easily affected by harmonics, so harmonic compensation technology is becoming more important. To solve this problem, an active power filter (APF) is an effective device widely used to improve power quality [1,2]. Working as a compensation circuit, the control method of APF has traditionally referred to control methods based on grid synchronization for distributed power generation systems [3]. Traditional PI control has the advantages of theory universality and has been widely used on many control targets [4]. In traditional control methods, Proportional Resonant (PR) controller is also one of the mainstreams [5]. Angulo et al. developed an implicit closed-loop current controller and resonant controller, which introduces the concept of a simplified model to reduce modeling complexity [6]. Yi et al. adopted the direction of the vector resonance to design a shunt active power filter control scheme, incorporating the idea of feedback control [7]. Fang et al. discussed the structure and parameter design of a resonant LCL filter and designed a novel filter to raise performance [8].

To deal with the more changeable situation due to modern load complexity, many scholars apply advanced control methods, especially adaptive methods, to improve the versatility and stability of APF. Wang et al. focused on the finiteness of switch states and designed a model predictive control scheme [9], achieving multi-objective control through a value function. Razmjooei et al. presented a novel framework for a time-varying observer design for a nonlinear system [10], then as a follow-up, proposed an adaptive fast-finite-time extended state observer, which raises the convergence rate [11], and offered an adaptive fast-finite-time extended state observer to further reduce the influence of the initial value [12]. An adaptive thyristor-controlled LC-Hybrid active power filter is proposed by Lam et al., whose main purpose is to reduce switching loss [13]. Lock et al. developed a one-cycle control strategy and used DSP as the hardware platform on a shunt active power filter [14], thus rejecting common-mode currents caused by common-mode voltages. Incremona et al. designed a sliding mode controller for nonlinear systems under strict constraints on the system and output [15]. Razmjooei et al. designed a disturbance observer-based backstepping tracking control to have more accuracy and faster convergence, reflecting the advantages of feedback control [16].

To deal with the model uncertainty caused by the mutual coupling of voltage and current in APF and high-order harmonics caused by the switching process, sliding mode control is often used owing to its versatility [17]. For example, a sliding mode controller combined with a vector operation technology for APF was proposed by Morales et al., which aimed at overcoming the coupling problem of traditional models [18]. In addition, a neural network is feasible for approximation on the nonlinear part [19,20]. As examples to show the flexibility of neural networks, a composite learning control of a flexible-link manipulator is designed using a neural network approximator [19], and a hybrid double hidden layer perceptron takes the form of a neural network [20]. Wai et al. introduced an adaptive FNN control for a single-stage boost inverter [21]. A recurrent neural network (RNN) controller combined with LCL filters was proposed by Fu and Li for grid-connected converters [22]. A continuous fractional-order nonsingular terminal sliding mode control was developed to track robot manipulators' control design [23]. A direct super-twisting power control method to control a brushless doubly-fed induction generator showed the adaptive sliding mode's contribution to reducing output oscillation [24]. A control method for a micro gyroscope was proposed to combine a sliding mode control and pattern recognition method [25]. The control methods above show that the combination of SMC and neural networks is efficient in dealing with an uncertain model.

For the neural networks, not all the features and data of the neurons have enough reference value. Moreover, the high-frequency signal change will lead to a significant decrease in reliability at some time points. Hence, to reduce redundant data, the feature selection methods came into being with high recognition ability and flexibility. An approach focused on a function approximation-type problem adopting the way of selecting the useful features and designing the rules based on the Takagi–Sugeno framework was proposed in [26], which gives a hint on how to deal with the situation when the original dimension of the input is very high. In [27], Padungweang et al. studied the probability density distribution on the Fourier transform and proposed an unsupervised discrimination analysis for feature selection. In [28], a global and local structure preservation framework for feature selection has been proposed. The framework conducted feature selection by integrating both global pairwise sample similarity and local geometric data structure. There are also some fuzzy neural controllers which make full use of the neural network to improve the control effect of complex models, reflecting the versatility and structural flexibility of neural networks [29–34].

Inspired by the methods mentioned above, this manufacturer proposes an adaptive super-twisting sliding mode control (STSMC) method for an active power filter based on a multi-feedback feature selection fuzzy neural network (MFFSFNN). Compared with the existing literature, the major contributions can be briefly summarized in the following outlines:

(1) Compared with traditional methods, the MFFSFNN-STSMC has the advantage of high adaptability and tolerance. Traditional methods will perform poorly when dealing

with the grid without enough accurate system information. However, with the sliding mode's low dependence on parameter accuracy and the neural network's approximation ability to unknown systems, the proposed method can deal with disturbances and model uncertainty resulting from changes in the external environment and internal structural errors.

(2) A feature selection layer is added to an output feedback neural network to attach the characteristics of signal filtering to the neural network. The signal filtering process can deal with fast-changing input signals of a wider range of amplitudes and helps the parameters and output converge quickly, thus improving training accuracy. In addition, choosing suitable process data as a learning object helps reduce computing burden and increase learning speed by reducing data redundancy. To realize the target, feature degree and evaluation function are added to the layer to evaluate whether and how to use the signals. These parameters have formal consistency with the parameters of the feedback neural network, so the complexity of the system does not increase significantly. Among them, feature degree is adaptively tuned to improve accuracy and reduce the difficulty of setting, thus maintaining the dynamic stability of the network structure and signal throughput. In addition, the signal filtering process also has a positive effect on countering external disturbance because of its versatility.

(3) An adaptive super-twisting sliding mode is used to assist in dealing with high-order harmonic problems and guarantee strong robustness. Compared with the traditional sliding mode, the adaptive gain of STSMC has the advantage of making the output smoother and helping extend the service life of the system. In addition, because it is a high-order sliding mode controller, it is less dependent on the accuracy of system information. At the same time, its adaptive nature helps reduce the dependence on the design of the sliding mode parameters.

2. Modeling of Active Power Filter

A single-phase APF mainly includes three parts: an AC power supply network called grid power, a non-linear load, and a DC side controller, which is the main circuit. In this paper, an inverter circuit with pulse width modulation as a direct control method is chosen as the main circuit, and a bridge circuit using IGBTs is used as a switching device. The actual diodes and other electronic components have parameter changes because of various factors such as temperature, extra resistance, and inductance added to the circuit to have a basic filtering effect. Though the filtering effect of this additional structure is not enough, the structure connects the AC and DC side and protects the system from extremely high currents. It also provides an important basis for system modeling. Therefore, it is also an important part of the system. In theory, capacitance is used as an energy supply element adopted in simulation. Because there is a necessity to leave a margin for the capacitance to charge, the error between the ideal DC side voltage and the actual value is also seen as a reference for current compensation in the system. Because the topic of the proposed method is harmonic compensation, which mostly concentrates on the steady state, in order to protect the circuit from huge instantaneous current, a regulated power supply is used as the DC side source in the experiment. Though the voltage will still change slightly because of the load change, the neural network has enough tolerance to deal with the slight change. To imitate load change in actual use, a single-phase uncontrollable rectifier bridge with variable load is settled, as shown in Figure 1.

Using Kirchhoff's voltage theory on the voltage loop of the AC side and main circuit, it can be obtained that

$$U_s = L\frac{di_c}{dt} + Ri_c + QU_{dc} \tag{1}$$

where U_s is the supply voltage, set as a sine wave, i_c represents a compensation current, U_{dc} is a DC-side capacitor voltage, and L and R are the link components in the main circuit of the active filter main circuit. Q is a switch function. Because extra components are already added, IGBT can be considered an ideal circuit. Then, define switch function Q as follows:

$$Q = \begin{cases} 1 & VT_1, VT_4\text{on}, \quad VT_2, VT_3off \\ -1 & VT_2, VT_3\text{on}, \quad VT_1, VT_4off \end{cases} \tag{2}$$

On the DC-side, the contribution of integral control to voltage stability is invalid, so proportional control is used, and the state equation of the compensation current is chosen as the main subject. The equation is written as follows:

$$\dot{i}_c = -\frac{R}{L}i_c + \frac{U_s}{L} - \frac{U_{dc}}{L}Q \tag{3}$$

Generally, it is necessary to have more and higher-level model information in order to design a higher-order controller to improve system performance. Therefore, the model of active power filter is usually considered a second-order model. Then, taking the derivative of Equation (3), obtains

$$\begin{aligned} \ddot{\mathrm{i}}_c &= -\tfrac{R}{L}\dot{i}_c + \tfrac{\dot{U}_s}{L} - \tfrac{\dot{U}_{dc}}{L}Q \\ &= -\tfrac{R}{L}(-\tfrac{R}{L}i_c + \tfrac{U_s}{L} - \tfrac{U_{dc}}{L}Q) + \tfrac{\dot{U}_s}{L} - \tfrac{\dot{U}_{dc}}{L}Q \\ &= \tfrac{R^2}{L^2}i_c + \tfrac{\dot{U}_s}{L} - \tfrac{R}{L^2}U_s + (\tfrac{R}{L^2}U_{dc} - \tfrac{\dot{U}_{dc}}{L})Q \end{aligned} \tag{4}$$

There is a problem in that Q is not perfectly constant, so on the turning point, the model does not work. But thanks to the fact that the turning point only lasts for an instant on the filtering effect of the inductance, it will not have a visibly bad effect on the system.

To get a standard model, Equation (4) can be sorted as

$$\ddot{\mathrm{x}} = \mathrm{f}(\mathrm{x}) + \mathrm{Bu} \tag{5}$$

where $x = i_c$, $f(x) = \frac{R^2}{L^2}i_c + \frac{\dot{U}_s}{L} - \frac{R}{L^2}U_s$, $B = \frac{R}{L^2}U_{dc} - \frac{\dot{U}_{dc}}{L}$, $u = Q$.

Due to the errors of internal parameters and external disturbances in actual use and the modeling error, the state equation inevitably has uncertainties. Finally, the target system can be summarized as

$$\ddot{\mathrm{x}} = \mathrm{f}(\mathrm{x}) + \mathrm{Bu}+\varphi(t) \tag{6}$$

where $\varphi(t)$ represents the lumped uncertainty.

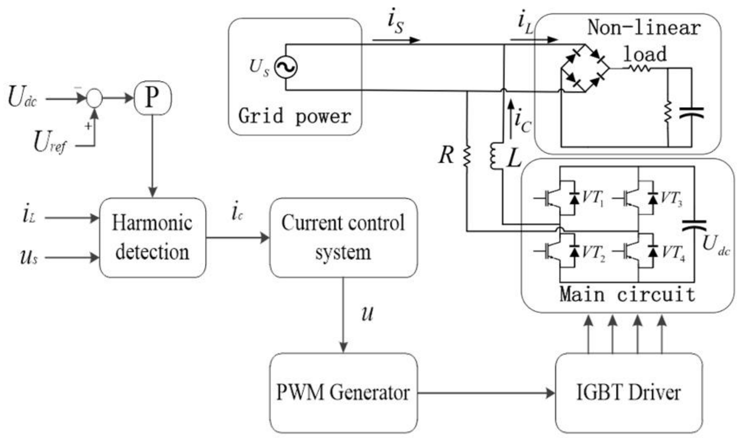

Figure 1. Structure of single-phase active power filter.

3. Structure of Multi-Feedback Feature Selection Fuzzy Neural Network

The multi-feedback feature selection fuzzy neural network can feed internal signals, external signals, and specific weight variables simultaneously so that the entire neural network has more information for reference. Using a fuzzy neural network instead of the traditional fuzzy method helps deal with the complexity of the APF system because, in the fuzzy neural network, fuzzy rule bases can be arranged adaptively, reducing manual dependence and improving its effectiveness. MFFSFNN has the advantage of adaptive feedback neural networks, the initial value whose related parameters can be set arbitrarily and have self-correction and self-optimization ability. By adding the feature selection layer to the neural network to filter the input signal, MFFSFNN has the ability to deal with the irregular high-frequency oscillating signal. This characteristic is effective in the APF control method for the inevitable current fluctuation of the PWM wave.

The structure of MFFSFNN is shown in Figure 2.

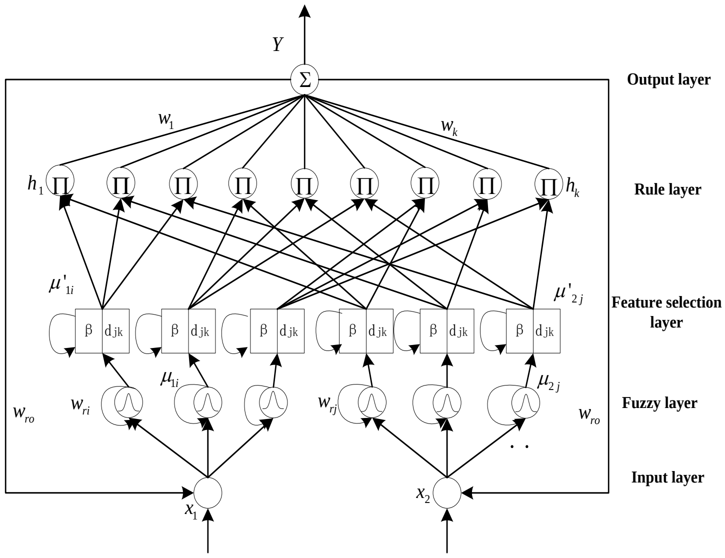

Figure 2. Structure of MFFSFNN.

(1) Input layer. Its main function is to combine the input $X = [x_1\ x_2 \dots x_m]^T$ and the previous round's output exY as the new input of the network to the next layer. Usually, variables related to power supply current are selected as the input, which is far smaller than the network output. Still, to keep the health of the learning process, the inputs should play a major role, so the input layer and the output layers are connected by the outer weights w_{ro} to cut the magnitude of exY. The output of this layer is $\theta = [\theta_1, \theta_2 \dots \theta_m]^T$.

$$\theta_m = x_m \cdot w_{rom} \cdot exY \tag{7}$$

(2) Fuzzy layer. This layer aims at calculating the membership. The Gaussian function is selected as the membership function. This layer can adaptively adjust the related parameter during the approximation process to reduce the dependence on the accuracy of the initial value. The output of this layer combines the output of the input layer and the feedback signal of the previous round of the fuzzy layer. Assume the nodes number is 3 $\mu_{1i}, \mu_{2j} \dots$ $(i = 1 \sim 3, j = 1 \sim 3)$; there are

$$\mu_{1i} = \exp[-\frac{\|\theta_1 + w_{ri} \cdot ex\mu_{1i} - c_{1i}\|^2}{b^2{}_{1i}}] \tag{8}$$

$$\mu_{2j} = \exp[-\frac{\|\theta_2 + w_{rj} \cdot ex\mu_{2j} - c_{2j}\|^2}{b^2{}_{2j}}] \tag{9}$$

where $w_{ri},\ w_{rj}$ are the internal feedback parameters, $c = [c_{11} \ldots c_{13}, c_{21} \ldots c_{23}]^T$ is the center vector, and $b = [b_{11} \ldots b_{13}, b_{21} \ldots b_{23}]^T$ is the base width. Considering the fact that inputs are fast-changing and the initial inputs are usually unstable, internal feedback is used to control the sensitivity of the fuzzy layer and study speed.

(3) Feature selection layer. The main purpose of this layer is to filter the input signal. This layer attaches a kind of feature degree to the inputs, judges their worth, and decides how to deal with them. Set the availability parameters as $\alpha_1(i)$ and α_2(j) there are

$$\begin{aligned} \alpha_{1i} &= 1 - \exp(-(\beta_{1i}\omega_{bi}ex\beta_{1i})^2) \\ \alpha_{2j} &= 1 - \exp(-(\beta_{2j}\omega_{bj}ex\beta_{2j})^2) \end{aligned} \tag{10}$$

where β is a feature degree, $ex\beta$ is the feature degree in the previous round, and ω_b is a recurrent weight. After obtaining the availability parameters, they would be compared with the system error level to determine whether it meets the current system requirements and save the results to the entry limit parameter d_i and d_j. The detailed function is expressed as

$$\begin{aligned} d_{1i} &= \begin{cases} M & \alpha_i \le T_e \\ 1 & \alpha_i > T_e \end{cases} \\ d_{2j} &= \begin{cases} M & \alpha_j \le T_e \\ 1 & \alpha_j > T_e \end{cases} \end{aligned} \tag{11}$$

where $T_e = \frac{1}{1+\mathrm{k}(x_1{}^2+x_2{}^2)}$ represents the system error level, working as the threshold. When using this function, there is a requirement that the optimal value of x is 0. M is the eigenvalue, which should meet the need of $1 \ne M \ne M^2$, x_1 and x_2 are two inputs for the system, and k is a positive constant to decide the strictness of the selection. The output of this layer is expressed as

$$\begin{aligned} \mu'_{1i} &= \mu_{1i}\alpha_{1i} \\ \mu'_{2j} &= \mu_{2j}\alpha_{2j} \end{aligned} \tag{12}$$

(4) Rule layer. This layer is used to determine whether and how to use the signal and decide the form of the output of this layer by judging the entry limit parameters. Each node in the rule layer is marked as $\prod$. This layer completes the comparison, selection, and multiplication of the input signal. The output of the rule layer is as follows:

$$h_k = \begin{cases} \mu'_{1i} \cdot \mu'_{2j} & d_{1i}d_{2j} \ne M \\ \max(\mu'_{1i}, \mu'_{2j}) & d_{1i}d_{2j} = M \end{cases} \tag{13}$$

where $k = 3 \times (i-1) + j, i = 1 \sim 3, j = 1 \sim 3, k = 1 \sim 9$. Among the two circumstances, $d_{1i}d_{2j} = M$ shows that there is only one input meeting the requirement. Because α, which is smaller than 1, is multiplied to μ, the bigger value usually meets the requirement. Therefore, the maximum value function is used to select the suitable output. $d_{1i}d_{2j} \ne M$ shows the two inputs, both or neither, meet the requirement. When they both meet the requirement, it is reasonable to use both of them, and in this situation, adding α to μ does not significantly influence the results for α, which is extremely close to 1. When neither, there are two circumstances. In the stable phase, because α is smaller, h_k in this situation should be smaller than those both meeting the requirement, and nodes of this kind should have a smaller influence on the final output. Therefore, it can also be used. In the early study phase, it is normal that all the inputs do not meet the requirements, but in this phase, this kind of data is needed to adjust the parameters of the neural network, so the inputs which do not meet the requirement are also required.

The manual of the feature selection layer, rule layer, and their connection method is shown in Figure 3b for reference.

(5) Output layer. This layer mainly uses a weighted average method to integrate the outputs of the rule layer to calculate the final result of the network. The output neuron is

connected with all the neurons in the rule layer through the weight $w = [w_1, w_2, \ldots, w_k]$. The signal node of the output layer is marked as $\sum$, which represents the calculation of all the inputs. The sum of the signals is expressed in the following form:

$$Y = \sum_{k=1}^{9} w_k h_k = w_1 h_1 + w_2 h_2 + \ldots + w_k h_k \tag{14}$$

Finally, the output feeds back to the input layer with the outer feedback weight w_{ro}.

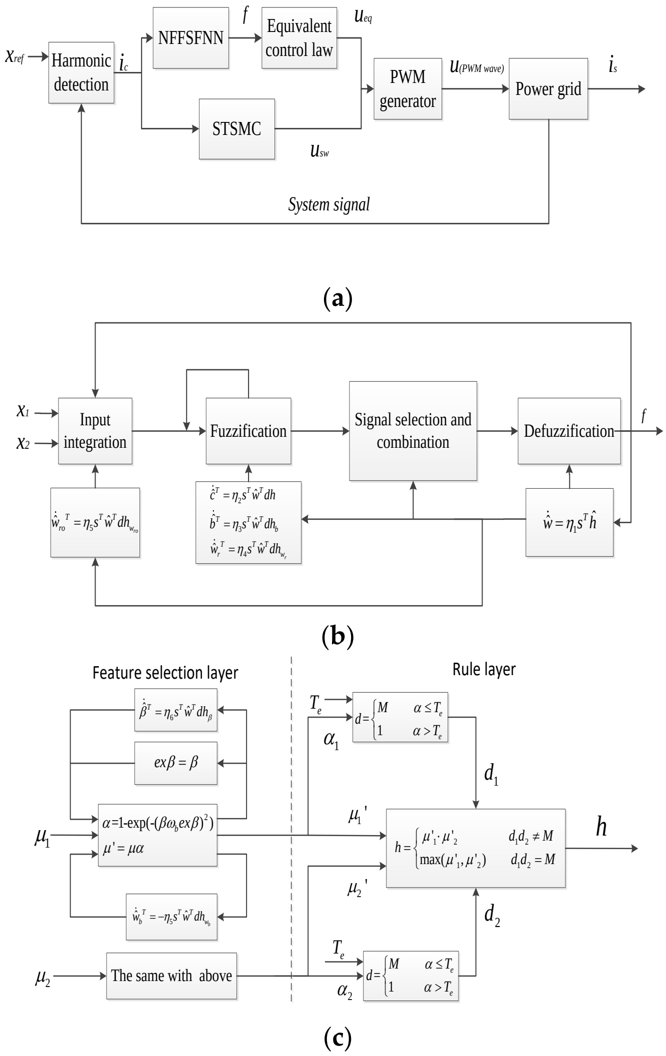

Figure 3. Block diagram of the proposed control method for APF: (**a**) Overall structure of the controller (**b**) Total study process of MFFSFNN (**c**) Detailed process of signal selection and combination process.

4. Controller Design and Stability Analysis

The configuration of the proposed control scheme is depicted in Figure 3, which mainly has two parts, including the MFFSFNN and STSMC methods. The MFFSFNN provides a solution to the unknown model and parameter uncertainty problem of the actual system by obtaining the system model through adaptive approximation, adding the advantage of low dependency on the precise parameters of the actual system to the control method. The STSMC is used to compensate for bias caused by neural networks.

Taking the uncertainty and disturbance into consideration, the APF system model is expressed as

$$\ddot{q} = f + Bu + \varphi(t) \tag{15}$$

The designed sliding surface is

$$s = ce + \dot{e} \tag{16}$$

where c is a sliding mode constant, $e, \dot{e}$ are the tracking error and its derivative, as

$$e = q - q_r \tag{17}$$

$$\dot{e} = \dot{q} - \dot{q}_r \tag{18}$$

Then,

$$\dot{s} = c\dot{e} + \ddot{e} = c\dot{e} + \ddot{q} - \ddot{q}_r \tag{19}$$

Substituting Equation (15) into Equation (19) yields

$$\dot{s} = c\dot{e} + f + B\mathrm{u} - \ddot{\mathrm{q}}_r + \varphi(t) \tag{20}$$

Considering there is no way to know the specific source, the specific value and influence of parameter uncertainty and disturbance cannot be considered a computable function, so ignore it for a while. When the sliding mode is in a steady state, where $\dot{s}$ converges to 0, the equivalent control law can be obtained as follows:

$$u_{eq} = \frac{1}{B}(\ddot{\mathrm{q}}_r - c\dot{e} - f) \tag{21}$$

STSMC is used as a compensator, widely used in the control method for its adaptability and smoothness. The switching control law is designed as

$$u_{sw} = -k_1\sqrt{|s|}\mathrm{sgn}(s) - \int k_2\mathrm{sgn}(s)dt \tag{22}$$

where k_1 and k_2 are positive constants, and $k_1 > \rho > |\varphi(t)|, k_2 > \delta > \left|\dot{\varphi}(t)\right|$. Among them ρ is the upper bound of system uncertainty and disturbance and δ is the upper bound of the change rate of system uncertainty and external disturbance.

Then the total control law u is

$$u = \frac{1}{B}(\ddot{\mathrm{q}}_r - c\dot{e} - f) - k_1\sqrt{|s|}\mathrm{sgn}(s) - \int k_2\mathrm{sgn}(s)dt \tag{23}$$

The neural network approximates the unknown model part f of the system, and the approximate result is $\hat{f}$, so in actual use, the control law can be rewritten as

$$u = \frac{1}{B}(\ddot{q}_r - c\dot{e} - \hat{f}) - k_1\sqrt{|s|}\mathrm{sgn}(s) - \int k_2\mathrm{sgn}(s)dt \tag{24}$$

where $\hat{f} = \hat{w}^T\hat{h}(x, \hat{c}, \hat{b}, \hat{w}_r, \hat{w}_b, \beta, \hat{w}_{ro})$.

To determine the error information and let the approximation result be smooth, set the first Lyapunov function as

$$V_1 = \frac{1}{2}s^2 \tag{25}$$

Then, its derivative can be obtained as

$$\begin{aligned}\dot{V}_1 &= s\dot{s} \\ &= s(c\dot{e} + f + Bu - \ddot{\mathrm{q}}_r + \varphi(t)) \\ &= s(f - \hat{f} - Bk_1\sqrt{|s|}\mathrm{sgn}(s) - Bk_2\textstyle\int \mathrm{sgn}(s)dt + \varphi(t))\end{aligned} \tag{26}$$

If the unknown model f is approximated successfully, the parameters will have their optimal values, set best weight as w^*, and similarly, best base width b^*, center vector c^*, inner feedback gain w_r^*, feature degree β^*, current parameter $\omega_b{}^*$ and outer feedback gain w_{ro}^*, then $f = w^{*T}h^* + \xi$, where $h^* = h^*(x, c^*, b^*, w_r^*, w_b^*, \beta, w_{ro}^*)$ and ξ is the mapping error.

Learning errors of the above-mentioned parameter are defined as

$$\begin{cases} \widetilde{h} = h^* - \hat{h} \\ \widetilde{w} = w^* - \hat{w} \\ \widetilde{b} = b^* - \hat{b} \\ \widetilde{c} = c^* - \hat{c} \\ \widetilde{w}_r = w_r^* - \hat{w}_r \\ \widetilde{w}_b = w_b^* - \hat{w}_b \\ \widetilde{\beta} = \beta^* - \hat{\beta} \\ \widetilde{w}_{ro} = w_{ro}^* - \hat{w}_{ro} \end{cases} \tag{27}$$

Therefore, the approximation error of the unknown part can be quantified as

$$\begin{aligned} f - \hat{f} &= w^{*T}h^* + \xi - \hat{w}^T\hat{h} \\ &= (w^{*T} - \hat{w}^T)\hat{h} + (\widetilde{w}^T + \hat{w}^T)\widetilde{h} + \xi \\ &= \widetilde{w}^T\hat{h} + \widetilde{w}^T\widetilde{h} + \hat{w}^T\widetilde{h} + \xi \end{aligned} \tag{28}$$

Define

$$\xi_0 = \widetilde{w}^T\widetilde{h} + \xi \tag{29}$$

Then Equation (28) becomes

$$f - \hat{f} = \widetilde{w}^T\hat{h} + \hat{w}^T\widetilde{h} + \xi_0 \tag{30}$$

In order to formulate the connection between the internal signals and parameters of the neural network, the Taylor expansion of $\widetilde{h}$ is performed, as

$$\begin{aligned} \widetilde{h} \quad &= \frac{\partial \widetilde{h}}{\partial c}\Big|_{|c=\hat{c}}(c^* - \hat{c}) + \frac{\partial \widetilde{h}}{\partial b}\Big|_{|b=\hat{b}}(b^* - \hat{b}) + \frac{\partial \widetilde{h}}{\partial w_r}\Big|_{|w_r=\hat{w}_r}(w_r^* - \hat{w}_r) \\ &+ \frac{\partial \widetilde{h}}{\partial w_b}\Big|_{|w_b=\hat{w}_b}(w_b^* - \hat{w}_b) + \frac{\partial \widetilde{h}}{\partial \beta}\Big|_{|\beta=\hat{\beta}}(\beta^* - \hat{\beta}) + \frac{\partial \widetilde{h}}{\partial w_{ro}}\Big|_{|w_{ro}=\hat{w}_{ro}}(w_{ro}^* - \hat{w}_{ro}) + O_h \\ &= dh_c \cdot \widetilde{c} + dh_b \cdot \widetilde{b} + dh_{w_r} \cdot \widetilde{w}_r \\ &+ dh_{w_b} \cdot \widetilde{w}_b + dh_\beta \cdot \widetilde{\beta} + dh_{w_{ro}} \cdot \widetilde{w}_{ro} + O_h \end{aligned} \tag{31}$$

where O_h represents higher-order terms. The coefficient matrix $dh_c, dh_b, dh_{w_r}, dh_{w_b}, dh_\beta, dh_{w_{ro}}$ is as follows:

$$\begin{cases} dh_c = \left[\frac{\partial \widetilde{h}_1}{\partial c}^T, \frac{\partial \widetilde{h}_2}{\partial c}^T \cdots \frac{\partial \widetilde{h}_k}{\partial c}^T \right]^T \Big|_{c=\hat{c}} \\ dh_b = \left[\frac{\partial \widetilde{h}_1}{\partial b}^T, \frac{\partial \widetilde{h}_2}{\partial b}^T \cdots \frac{\partial \widetilde{h}_k}{\partial b}^T \right]^T \Big|_{b=\hat{b}} \\ dh_{w_r} = \left[\frac{\partial \widetilde{h}_1}{\partial w_r}^T, \frac{\partial \widetilde{h}_2}{\partial w_r}^T \cdots \frac{\partial \widetilde{h}_k}{\partial w_r}^T \right]^T \Big|_{w_r=\hat{w}_r} \\ dh_{w_b} = \left[\frac{\partial \widetilde{h}_1}{\partial w_b}^T, \frac{\partial \widetilde{h}_2}{\partial w_b}^T \cdots \frac{\partial \widetilde{h}_k}{\partial w_b}^T \right]^T \Big|_{w_b=\hat{w}_b} \\ dh_\beta = \left[\frac{\partial \widetilde{h}_1}{\partial \beta}^T, \frac{\partial \widetilde{h}_2}{\partial \beta}^T \cdots \frac{\partial \widetilde{h}_k}{\partial \beta}^T \right]^T \Big|_{\beta=\hat{\beta}} \\ dh_{w_{ro}} = \left[\frac{\partial \widetilde{h}_1}{\partial w_{ro}}^T, \frac{\partial \widetilde{h}_2}{\partial w_{ro}}^T \cdots \frac{\partial \widetilde{h}_k}{\partial w_{ro}}^T \right]^T \Big|_{w_{ro}=\hat{w}_{ro}} \end{cases} \tag{32}$$

Substituting Equation (31) into Equation (30) yields

$$\begin{aligned} f-\hat{f} &= \hat{w}^T(dh_c\cdot\tilde{c}+dh_b\cdot\tilde{b}+dh_{w_r}\cdot\tilde{w}_r+dh_{w_b}\cdot\tilde{w}_b \\ &\quad +dh_\beta\cdot\tilde{\beta}+dh_{w_{ro}}\cdot\tilde{w}_{ro}+O_h)+\xi_0+\tilde{w}^T\hat{h} \\ &= \hat{w}^T(dh_c\cdot\tilde{c}+dh_b\cdot\tilde{b}+dh_{w_r}\cdot\tilde{w}_r+dh_{w_b}\cdot\tilde{w}_b \\ &\quad +dh_\beta\cdot\tilde{\beta}+dh_{w_{ro}}\cdot\tilde{w}_{ro})+\hat{w}^TO_h+\xi_0+\tilde{w}^T\hat{h} \end{aligned} \tag{33}$$

Define total approximation error as $O_m=\hat{w}^TO_h+\xi_0$. It can be seen that the neural network method will have inevitable errors for its approaching mapping method and fuzzy method. Therefore, as a result, a compensator like STSMC used here is necessary.

Choose the Lyapunov function as

$$\begin{aligned} V &= \tfrac{1}{2}s^2+\tfrac{1}{2\eta_1}\tilde{w}^T\tilde{w}+\tfrac{1}{2\eta_2}\tilde{c}^T\tilde{c}+\tfrac{1}{2\eta_3}\tilde{b}^T\tilde{b} \\ &\quad +\tfrac{1}{2\eta_4}\tilde{w}_r^T\tilde{w}_r+\tfrac{1}{2\eta_5}\tilde{w}_b^T\tilde{w}_b+\tfrac{1}{2\eta_6}\tilde{\beta}^T\tilde{\beta}+\tfrac{1}{2\eta_7}\tilde{w}_{ro}^T\tilde{w}_{ro} \end{aligned} \tag{34}$$

Then, the derivative of Equation (34) can be obtained as

$$\begin{aligned} \dot{V} &= \dot{V}_1+\tfrac{1}{\eta_1}\tilde{w}^T\dot{\tilde{w}}+\tfrac{1}{\eta_2}\dot{\tilde{c}}^T\tilde{c}+\tfrac{1}{\eta_3}\dot{\tilde{b}}^T b+\tfrac{1}{\eta_4}\dot{\tilde{w}}_r^T\tilde{w}_r \\ &\quad +\tfrac{1}{\eta_5}\dot{\tilde{w}}_b^T\tilde{w}_b+\tfrac{1}{\eta_6}\dot{\tilde{\beta}}^T\tilde{\beta}+\tfrac{1}{\eta_7}\dot{\tilde{w}}_{ro}^T\tilde{w}_{ro} \\ &= s(f-\hat{f}-Bk_1\sqrt{|s|}\operatorname{sgn}(s)-Bk_2\textstyle\int\operatorname{sgn}(s)dt+\varphi(t)) \\ &\quad +\tfrac{1}{\eta_1}\tilde{w}^T\dot{\tilde{w}}+\tfrac{1}{\eta_2}\dot{\tilde{c}}^T\tilde{c}+\tfrac{1}{\eta_3}\dot{\tilde{b}}^T\tilde{b}+\tfrac{1}{\eta_4}\dot{\tilde{w}}_r^T\tilde{w}_r \\ &\quad +\tfrac{1}{\eta_5}\dot{\tilde{w}}_b^T\tilde{w}_b+\tfrac{1}{\eta_6}\dot{\tilde{\beta}}^T\tilde{\beta}+\tfrac{1}{\eta_7}\dot{\tilde{w}}_{ro}^T\tilde{w}_{ro} \end{aligned} \tag{35}$$

Substituting Equation (33) into Equation (35) yields

$$\begin{aligned} \dot{V} = {} & s\tilde{w}^T\hat{h}+\tfrac{1}{\eta_1}\tilde{w}^T\dot{\tilde{w}}+s\hat{w}^Tdh_c\cdot\tilde{c}+\tfrac{1}{\eta_2}\dot{\tilde{c}}^T\tilde{c}+s\hat{w}^Tdh_b\cdot\tilde{b}+\tfrac{1}{\eta_3}\dot{\tilde{b}}^T\tilde{b} \\ & +s\hat{w}^Tdh_{w_r}\cdot\tilde{w}_r+\tfrac{1}{\eta_4}\dot{\tilde{w}}_r^T\tilde{w}_r+s\hat{w}^Tdh_{w_b}\cdot\tilde{w}_b+\tfrac{1}{\eta_5}\dot{\tilde{w}}_b^T\tilde{w}_b \\ & +s\hat{w}^Tdh_\beta\cdot\tilde{\beta}+\tfrac{1}{\eta_6}\dot{\tilde{\beta}}^T\tilde{\beta}+s\hat{w}^Tdh_{w_{ro}}\cdot\tilde{w}_{ro}+\tfrac{1}{\eta_7}\dot{\tilde{w}}_{ro}^T\tilde{w}_{ro} \\ & +sO_m-Bk_1s\sqrt{|s|}\operatorname{sgn}(s)-Bk_2s\textstyle\int\operatorname{sgn}(s)dt+s\varphi(t) \end{aligned} \tag{36}$$

Let $s^T\tilde{w}^T\hat{h}+\frac{1}{\eta_1}\tilde{w}^T\dot{\tilde{w}}=0$, it can be obtained that

$$\dot{\tilde{w}}=-\dot{\hat{w}}=-\eta_1s^T\hat{h} \tag{37}$$

Similarly, other adaptation laws can be obtained, and finally, the adaptation laws can be derived as

$$\begin{cases} \dot{\tilde{w}}=-\dot{\hat{w}}=-\eta_1s^T\hat{h} \\ \dot{\tilde{c}}^T=-\dot{\hat{c}}^T=-\eta_2s^T\hat{w}^Tdh_c \\ \dot{\tilde{b}}^T=-\dot{\hat{b}}^T=-\eta_3s^T\hat{w}^Tdh_b \\ \dot{\tilde{w}}_r{}^T=-\dot{\hat{w}}_r{}^T=-\eta_4s^T\hat{w}^Tdh_{w_r} \\ \dot{\tilde{w}}_b{}^T=-\dot{\hat{w}}_b{}^T=-\eta_5s^T\hat{w}^Tdh_{w_b} \\ \dot{\tilde{\beta}}^T=-\dot{\hat{\beta}}^T=-\eta_6s^T\hat{w}^Tdh_\beta \\ \dot{\tilde{w}}_{ro}{}^T=-\dot{\hat{w}}_{ro}{}^T=-\eta_7s^T\hat{w}^Tdh_{w_{ro}} \end{cases} \tag{38}$$

Substituting Equation (38) into Equation (36) yields

$$\begin{aligned} \dot{V} &= s(O_m - Bk_1\sqrt{|s|}\mathrm{sgn}(s) - Bk_2\int \mathrm{sgn}(s)dt + \varphi(t)) \\ &= -Bk_1|s|\sqrt{|s|} - B|s|\int k_2 dt + s\varphi(t) + sO_m \\ &\leq -Bk_1|s|\sqrt{|s|} - B|s|\int k_2 dt + |s||\varphi(t)| + |s||O_m| \\ &= -Bk_1|s|\sqrt{|s|} - |s|\int (Bk_2 - |\dot{\varphi}(t)| - \left|\dot{O}_m\right|)dt \end{aligned} \tag{39}$$

Suppose that O_m and its derivative are bounded, $\left|\dot{O}_m\right| \leq O_d$, where O_d is a positive constant. Similarly, suppose $\left|\dot{\varphi}(t)\right| \leq \delta$, where δ is a positive constant. Then, Equation (39) can be interfered as

$$\dot{V} \leq -Bk_1|s|\sqrt{|s|} - |s|\int (Bk_2 - \delta - O_d)dt \tag{40}$$

So, if there is k_2 which fits the condition $k_2 \geq \frac{1}{B}(\delta + O_d)$, it can be proved that

$$\dot{V} \leq -Bk_1|s|\sqrt{|s|} \leq 0 \tag{41}$$

Thus,

$$\int_0^t |s|^{\frac{3}{2}} dt \leq -\frac{1}{Bk_1}(V(t) - V(0)) \tag{42}$$

Since $V(0)$ and $V(t)$ are bounded because $V(t) > 0$ and $\dot{V}(t) \leq 0$, it can be concluded that $\lim\limits_{t\to\infty}\int_0^t |s|^{\frac{3}{2}} dt$ is bounded. With the condition that $\dot{s}$ is bounded and Barbalat's lemma, $s(t)$ will asymptotically converge to zero. Since $s(t)$ converge to zero, e will eventually tend to zero. Thus, the designed controller ensures the asymptotic stability of the closed-loop control system.

5. Simulation Study

To explore the feasibility and practical effect of the proposed method, this paper conducted a simulation experiment in MATLAB. The circuit's main parameters are set as in Table 1. To show the adaptive ability of MFFSFNN, the circuit increase a set of dynamic loads at 0.3 s; the initial values of the parameters are set as 1, except w_{ro}, which is set as 0. $\eta_1, \eta_2, \eta_3, \eta_4, \eta_5, \eta_6, \eta_7$ are set as $5 \times 10^9, 10^{-9}, 10^{-9}, 10^{-9}, 10^{-9}, 10^{-9}, 10^{-10}$, respectively. k_1 and k_2 are set as 3 and 4, respectively.

Table 1. Simulation parameters of APF.

Name	Parameter Value
Single-phase voltage RMS	24 V/50 Hz
Steady-state load	R_1 = 5 Ω, R_2 = 15 Ω, C = 10^{-3} F
Dynamic load	R_1 = 15 Ω, R_2 = 15 Ω, C = 10^{-3} F
Main circuit parameters	L = 1.8 × 10^{-2} H, R = 1 Ω, V_{ref} = 50 V
Sample time	10^{-5} s
Switching frequency	10 kHz

Figures 4 and 5 are the simulation output when the system is directly affected by harmonics. Because of the distortion of load current and nonlinear load, the power supply current cannot maintain a perfectly sinusoidal wave, especially on the top. As a result, total harmonic distortion (THD) is up to 13.04%, showing that the power quality is largely influenced and emphasizing the necessity for compensation.

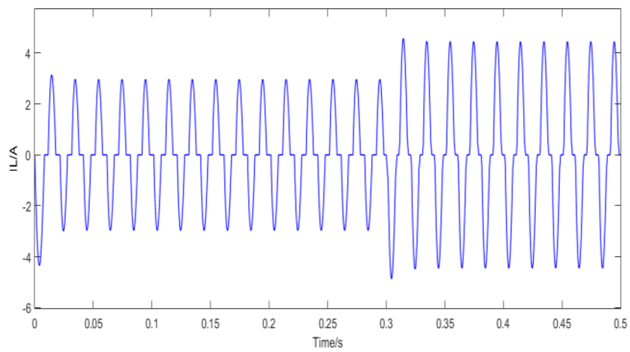

Figure 4. Distorted load current caused by load change.

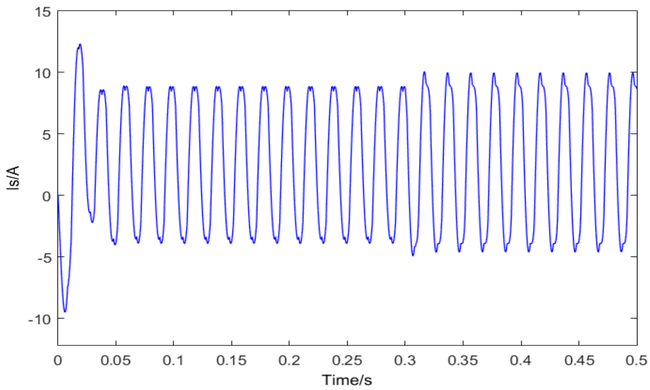

Figure 5. Power supply current influenced by load change.

Then, Figure 6 to Figure 7 is the system output with the proposed control method. Figure 5 is the tracking curve of compensation current with the error curve. The magnitude of the error is within ± 0.1, showing good tracking performance using the control method. Figure 5 is the controller output, where U_{eq} and U_{sw} have similar amplitude, showing that the neural network and sliding mode control have their part in this control method.

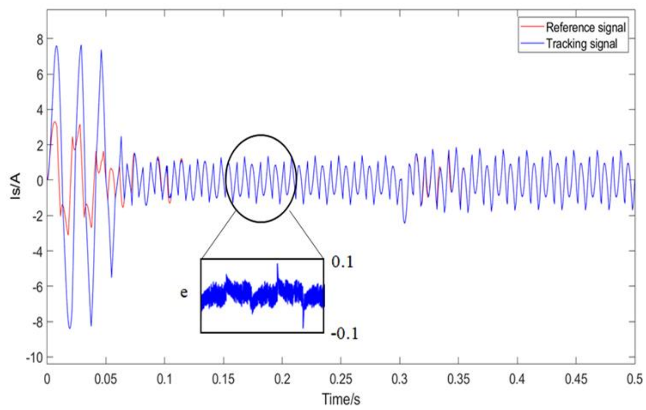

Figure 6. Tracking curve and local error magnification of compensation current.

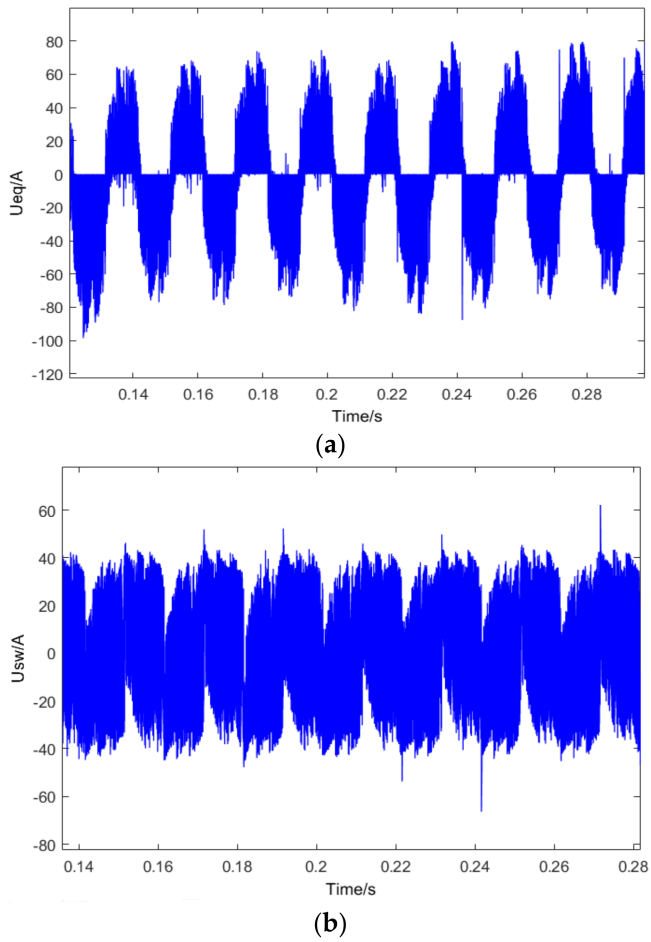

Figure 7. Controller output (**a**) Ueq, (**b**) Usw.

As shown in Figure 8, with the control of the proposed method, the power supply current can maintain a sinusoidal wave form through short-time adjustment. The output of MFFSFNN is shown in Figure 9, from which it can be seen that the learning process takes about 0.1 s. Considering the fact that the capacitance working as the DC power supply needs 0.15 s to charge, the learning process is short enough. Figure 10 shows that the THD is 1.48%, indicating that the method has an excellent control effect for harmonic problems and greatly contributes to improving power quality.

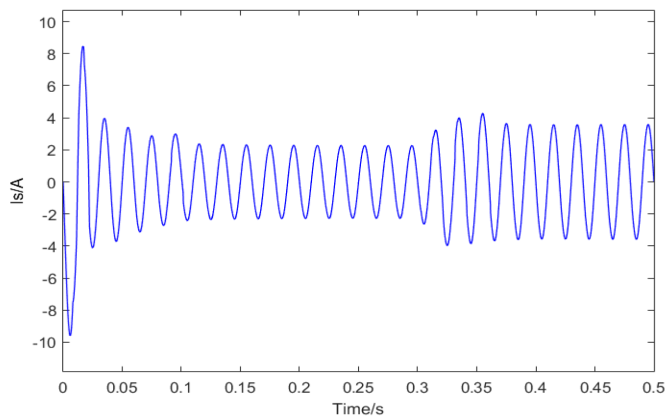

Figure 8. Power supply current with compensation of MFFSFNN-STSMC.

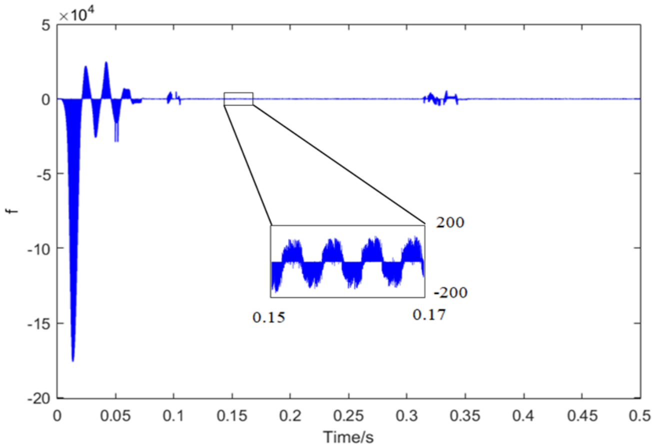

Figure 9. Output and error magnification of MFFSFNN.

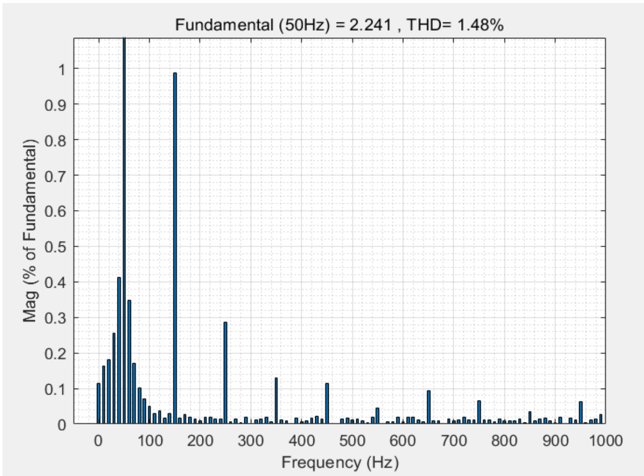

Figure 10. Spectrum analysis chart of power supply current.

An advanced algorithm recently published [35] is taken as a comparison. The comparative result is in Table 2, proving the superiority of the MFFSFNN-STSMC method.

Table 2. Performance comparison in simulation.

	MFFSFNN-STSMC	**OFFNN**
Steady-state load	1.48%	2.84%
With dynamic load	1.35%	2.44%

6. Experimental Verification

To prove that the application scope of this method is not limited to simulation, a dSPACE DS1104 single-phase APF prototype was built, and a series of hardware experiments were carried out. Figure 1 shows the structure of the single-phase APF experimental model. In addition to APF, the model also has signal acquisition circuits, main controller systems, IGBT drivers, and PWM generators. The function of the signal acquisition circuit is to acquire needed signals, where load current, the compensation current, power supply voltage, and DC side capacitor voltage are required for this example. After digitization, these signals are sent to the control system (in dSPACE DS1104). The error in the A/D conversion of the A/D conversion unit is 0.7% according to sensor selection, and the response time is 40µs, which fully meets the switching frequency requirements. Then, the controller sends control information to the PWM generator and drives the IGBT switch for current compensation. The load uses two sets representing steady-state and dynamic load, respectively, and are connected in parallel. The dynamic load is attached with a switch to imitate load change.

Figure 11 is the experimental prototype, where the setup mainly includes the part shown in Figure 1. The AC side current simulates harmonics. A programmable power source is used to simulate AC power with harmonics. The DC power supply is used to provide voltage on the DC side. The signals detected are I_S, I_L, U_{dc}, and U_s. The reference voltage and ideal signals are set in dSPACE instead of using another ideal signal generator.

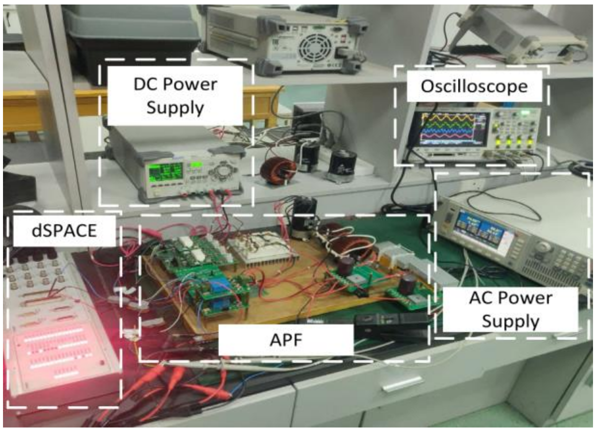

Figure 11. Experimental prototype.

6.1. Steady-State Experiment

Figure 12 is the output and oscilloscope harmonic distortion results in the steady state. In Figure 12a, the AC side supply voltage, load current, compensation current, and AC side supply current are from above to below. It can be seen that with compensation, though the load current has a severe dead zone phenomenon, the power supply current remains smooth. It can also be seen from Figure 12b that the THD change after compensation is 3.40%, which shows that the proposed control method still has sufficient harmonic compensation performance. For comparison, the results of four contrast algorithms from [36] and [8] are shown in Table 3. It can be proved that the proposed method has performance advantages compared with traditional filtering methods and other neural network methods.

Table 3. Comparison of THD in the experiment.

Control Method \ Performance	THD
MFFSFNN-STSMC	3.40%
ABNNCSMC	6.05%
ANNSMC	6.48%
LCL	5.16%
LLCL	4.40%

The results obtained in the hardware experiment are a bit poorer than those in the simulation because the time delay in the experiment is more serious than that in the simulation, and harmonic detection is sensitive to it according to instantaneous reactive power compensation theory. Though in simulation results, the THD of the proposed method is about 0.2% higher than that of ABNNCSMC, which is provided in [30]. In experiments, MFFSFNN-STSMC has better performance, demonstrating the robustness of the proposed method against delays and other external influences.

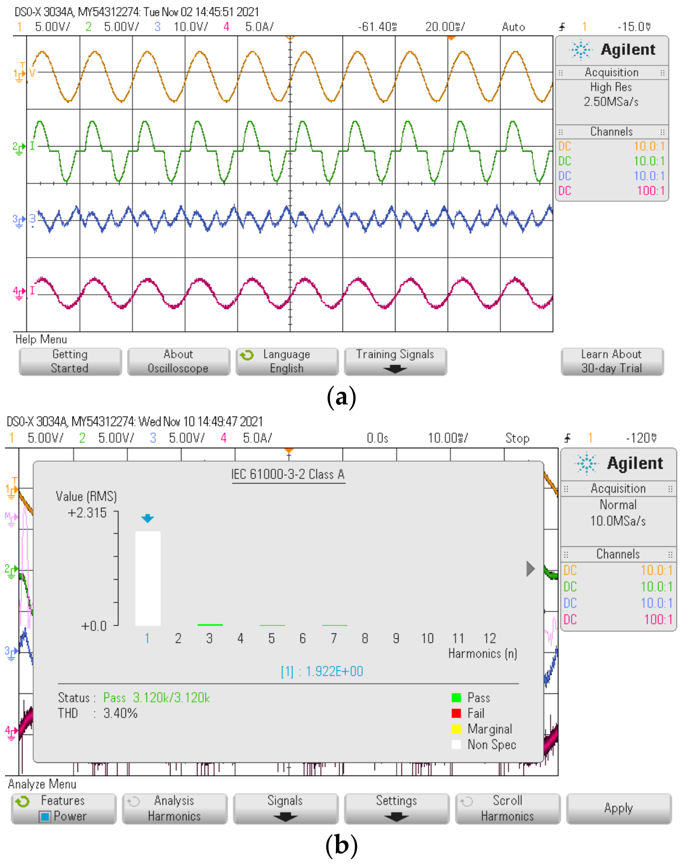

Figure 12. Experiments of steady state: (**a**) Signal curve (**b**) Harmonic spectrum of source current.

6.2. Dynamic Experiment of Load Change

Considering the sudden changes in the number or performance of user appliances in actual use, in order to prove the usability of the proposed method in actual use, an experiment on increasing and decreasing nonlinear load is set to imitate the load mutation. Figure 13 shows the situation with the load surge, and Figure 14 shows the opposite. In both situations, the waveform of the power supply current has changed slightly due to the change in the system environment. In addition, thanks to the self-adaptive ability of the proposed method, it reverts to standard in no time. THD is 3.16% and 3.60%, close to that of steady state (3.40%). It shows that the control system will change with the active change of load to maintain the control performance of the system, showing the robustness and control ability of the proposed method for complex and uncertain systems.

As a result, the simulation and experiment show that the proposed method has high robustness, adaptive ability, and rapidity and has been proven practical in experiments. However, when it comes to practical uses, the computational complexity of the proposed method is too high for most site controllers. dSPACE here has enough calculation speed, but in most sites, the controller is inferior, so the calculation and approximation process will be slowed down, resulting in a decline in timeliness. A method under test now is splitting the study and control processes, using computers of higher specifications to do the study process and transmit to the scene of the site controller. Ways of reducing computational complexity are also under discussion.

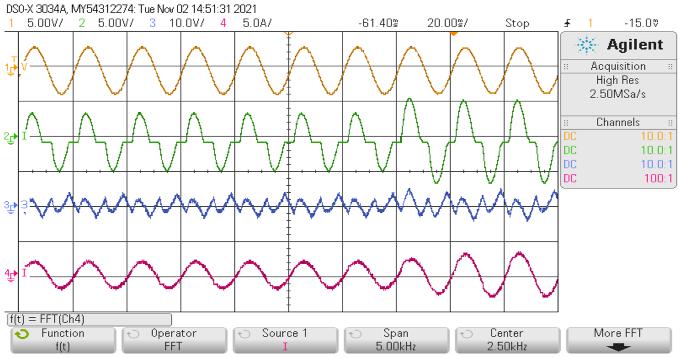

(**a**)

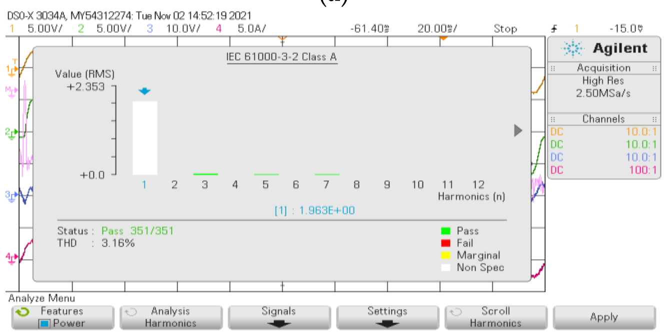

(**b**)

Figure 13. Experiments when increasing loads: (**a**) Signal curve (**b**) Harmonic spectrum of source current.

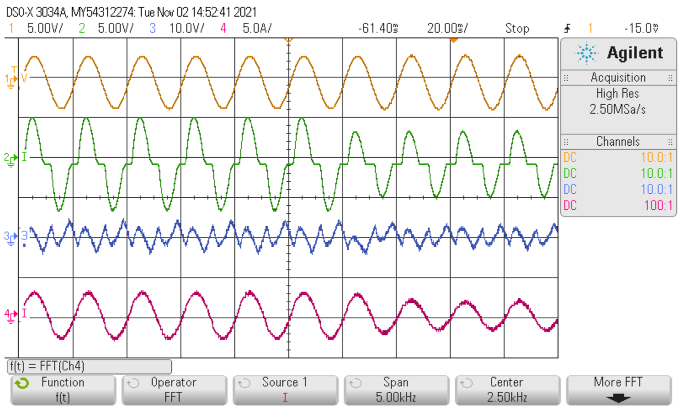

(**a**)

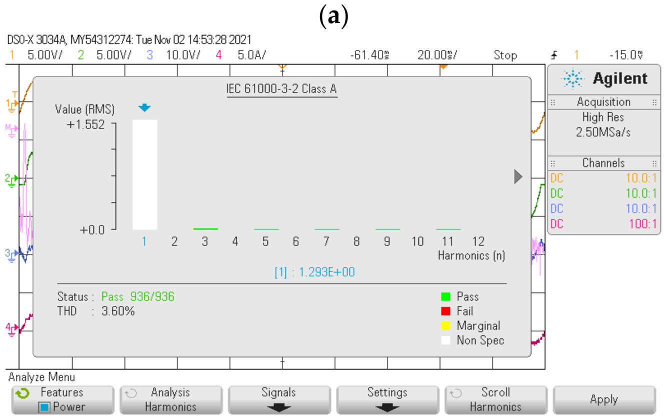

(**b**)

Figure 14. Experiments when decreasing loads: (**a**) Signal curve (**b**) Harmonic spectrum of source current.

7. Conclusions

This paper proposes a novel adaptive neural network method with a super-twisting sliding mode compensator for an active power filter. The proposed neural network has the advantage of tracking unknown parts of APF precisely and quickly. Furthermore, because of its feature selection characteristics and feedback, it has the advantage of self-adaption and processing capacity on fast-changing signals than traditional neural networks. STSMC is used to compensate for the approximation error of MFSFNN with its high versatility and suppress chatting in the system. Simulation and experimental results prove that the proposed method can achieve satisfactory performance in harmonic compensation when faced with system uncertainty and load changes.

In the future, authors will work on the proposed method's experimental verification on three-phase APF and in a high-voltage environment to prove the effectiveness of the method. In addition, a study on reducing the computational complexity of the actual system is in progress.

Author Contributions: Conceptualization, J.F.; Software, Q.P., Y.Z.; Validation, Q.P., Y.Z.; Formal analysis, Q.P.; Writing—original draft, Q.P.; Writing—review & editing, J.F.; Project administration, J.F. All authors have read and agreed to the published version of the manuscript.

Funding: This work is partially supported by the National Science Foundation of China under Grant No. 62273131.

Conflicts of Interest: The authors declare no conflict of interest.

References

1. Panigrahi, R.; Subudhi, B.; Panda, P. Model predictive-based shunt active power filter with a new reference current estimation strategy. *IET Power Electron.* **2015**, *8*, 221–233. [CrossRef]
2. Lascu, C.; Asiminoaei, L.; Boldea, I.; Blaabjerg, F. High performance current controller for selective harmonic compensation in active power filters. *IEEE Trans. Power Electron.* **2007**, *22*, 1826–1835. [CrossRef]
3. Blaabjerg, F.; Teodorescu, R.; Liserre, M.; Timbus, A.V. Overview of control and grid synchronization for distributed power generation systems. *IEEE Trans. Ind. Electron.* **2006**, *53*, 1398–1409. [CrossRef]
4. Costa, B.; Bacon, V.; Silva, S.; Angélico, B. Tuning of a PI-MR controller based on differential evolution metaheuristic applied to the current control loop of a shunt-APF. *IEEE Trans. Ind. Electron.* **2017**, *64*, 4751–4761. [CrossRef]
5. Mattavelli, P.; Marafao, F. Repetitive-based control for selective harmonic compensation in active power filters. *IEEE Trans. Ind. Electron.* **2004**, *51*, 1018–1024. [CrossRef]
6. Angulo, M.; Ruiz-Caballero, D.A.; Lago, J.; Heldwein, M.L.; Mussa, S.A. Active power filter control strategy with implicit closed-loop current control and resonant controller. *IEEE Trans. Ind. Electron.* **2013**, *60*, 2721–2730. [CrossRef]
7. Yi, H.; Zhuo, F.; Zhang, Y.; Li, Y.; Zhan, W.; Chen, W.; Liu, J. A source-current-detected shunt active power filter control scheme based on vector resonant controller. *IEEE Trans. Ind. Appl.* **2014**, *50*, 1953–1965. [CrossRef]
8. Fang, J.; Xiao, G.; Yang, X.; Tang, Y. Parameter design of a novel series-parallel-resonant LCL filter for single-phase half-bridge active power filters. *IEEE Trans. Power Electron.* **2017**, *32*, 200–217. [CrossRef]
9. Wang, R.; Hu, B.; Sun, S.; Man, F.; Yu, Z.; Chen, Q. Linear active disturbance rejection control for DC side voltage of single-phase active power filters. *IEEE Access* **2019**, *7*, 73095–73105. [CrossRef]
10. Razmjooei, H.; Palli, G.; Abdi, E. Continuous finite-time extended state observer design for electro-hydraulic systems. *J. Frankl. Inst.* **2022**, *359*, 5036–5055. [CrossRef]
11. Razmjooei, H.; Palli, G.; Janabi-Sharifi, F.; Alirezaee, S. Adaptive fast-finite-time extended state observer design for uncertain electro-hydraulic systems. *Eur. J. Control.* **2023**, *69*, 100749. [CrossRef]
12. Razmjooei, H.; Palli, G.; Abdi, E.; Terzo, M.; Strano, S. Design and experimental validation of an adaptive fast-finite-time observer on uncertain electro-hydraulic systems. *Control. Eng. Pr.* **2023**, *131*, 105391. [CrossRef]
13. Lam, C.-S.; Wang, L.; Ho, S.-I.; Wong, M.-C. Adaptive thyristor-controlled LC-hybrid active power filter for reactive power and current harmonics compensation with switching loss reduction. *IEEE Trans. Power Electron.* **2017**, *32*, 7577–7590. [CrossRef]
14. Lock, A.S.; da Silva, E.R.C.; Elbuluk, M.E.; Fernandes, D.A. An APF-OCC strategy for common-mode current rejection. *IEEE Trans. Ind. Appl.* **2016**, *52*, 4935–4945. [CrossRef]
15. Incremona, G.P.; Rubagotti, M.; Ferrara, A. Sliding mode control of constrained nonlinear systems. *IEEE Trans. Autom. Control* **2017**, *62*, 2965–2972. [CrossRef]
16. Razmjooei, H.; Palli, G.; Nazari, M. Disturbance observer-based nonlinear feedback control for position tracking of electro-hydraulic systems in a finite time. *Eur. J. Control.* **2022**, *67*, 100659. [CrossRef]

17. Young, K.; Utkin, V.; Ozguner, U. A control engineer's guide to sliding mode control. *IEEE Trans. Control Syst. Technol.* **1999**, *7*, 328–342. [CrossRef]
18. Morales, J.; Vicuña, L.; Guzman, R.; Castilla, M.; Miret, J. Modeling and sliding mode control for three-phase active power filters using the vector operation technique. *IEEE Trans. Ind. Electron.* **2018**, *65*, 6828–6838. [CrossRef]
19. Xu, B. Composite learning control of flexible-link manipulator using NN and DOB. *IEEE Trans. Syst. Man Cybern. Syst.* **2018**, *48*, 1979–1985. [CrossRef]
20. Fei, J.; Chen, Y. Fuzzy double hidden layer recurrent neural terminal sliding mode control of single-phase active power filter. *IEEE Trans. Fuzzy Syst.* **2021**, *29*, 3067–3081. [CrossRef]
21. Wai, R.-J.; Lin, Y.-F.; Liu, Y.-K. Design of adaptive fuzzy-neural-network control for a single-stage boost inverter. *IEEE Trans. Power Electron.* **2015**, *30*, 7282–7298. [CrossRef]
22. Fu, X.; Li, S. Control of single-phase grid-connected converters with LCL filters using recurrent neural network and conventional control methods. *IEEE Trans. Power Electron.* **2016**, *31*, 5354–5364. [CrossRef]
23. Wang, Y.; Gu, L.; Xu, Y.; Cao, X. Practical tracking control of robot manipulators with continuous fractional-order nonsingular terminal sliding mode. *IEEE Trans. Ind. Electron.* **2016**, *63*, 6194–6204. [CrossRef]
24. Sadeghi, R.; Madani, S.M.; Ataei, M.; Kashkooli, M.A.; Ademi, S. Super-twisting sliding mode direct power control of a brushless doubly fed induction generator. *IEEE Trans. Ind. Electron.* **2018**, *65*, 9147–9156. [CrossRef]
25. Fei, J.; Feng, Z. Fractional-order finite-time super-twisting sliding mode control of micro gyroscope based on double-loop fuzzy neural network. *IEEE Trans. Syst. Man Cybern. Syst.* **2021**, *51*, 7692–7706. [CrossRef]
26. Pal, N.R.; Saha, S. Simultaneous structure identification and fuzzy rule generation for takagi–sugeno models. *IEEE Trans. Syst. Man Cybern. Part B Cybern.* **2008**, *38*, 1626–1638. [CrossRef]
27. Padungweang, P.; Lursinsap, C.; Sunat, K. A discrimination analysis for unsupervised feature selection via optic diffraction principle. *IEEE Trans. Neural Netw. Learn. Syst.* **2012**, *23*, 1587–1600. [CrossRef] [PubMed]
28. Liu, X.; Wang, L.; Zhang, J.; Yin, J.; Liu, H. Global and local structure preservation for feature selection. *IEEE Trans. Neural Networks Learn. Syst.* **2014**, *25*, 1083–1095. [CrossRef]
29. Fei, J.; Wang, Z.; Pan, Q. Self-Constructing fuzzy neural fractional-order sliding mode control of active power filter. *IEEE Trans. Neural Netw. Learn. Syst.* **2022**, 1–12. [CrossRef] [PubMed]
30. Xu, B.; Zhang, R.; Li, S.; He, W.; Shi, Z. Composite neural learning-based nonsingular terminal sliding mode control of MEMS gyroscopes. *IEEE Trans. Neural Netw. Learn. Syst.* **2020**, *31*, 1375–1386. [CrossRef]
31. Fei, J.; Wang, Z.; Fang, Y. Self-evolving chebyshev fuzzy neural fractional-order sliding mode control for active power filter. *IEEE Trans. Ind. Inform.* **2023**, *19*, 2729–2739. [CrossRef]
32. Fei, J.; Chen, Y.; Liu, L.; Fang, Y. Fuzzy multiple hidden layer recurrent neural control of nonlinear system using terminal sliding-mode controller. *IEEE Trans. Cybern.* **2022**, *52*, 9519–9534. [CrossRef] [PubMed]
33. Li, Y.; Zhang, J.; Liu, W.; Tong, S. Observer-based adaptive optimized control for stochastic nonlinear systems with input and state constraints. *IEEE Trans. Neural Netw. Learn. Syst.* **2021**, *33*, 7791–7805. [CrossRef]
34. Fei, J.; Wang, H.; Fang, Y. Novel neural network fractional-order sliding mode control with application to active power filter. *IEEE Trans. Syst. Man Cybern. Syst.* **2022**, *52*, 3508–3518. [CrossRef]
35. Pan, Q.; Li, X.; Fei, J. Adaptive fuzzy neural network harmonic control with a super-twisting sliding mode approach. *Mathematics* **2022**, *10*, 1063. [CrossRef]
36. Fei, J.; Liu, N.; Hou, S.; Fang, Y. Neural network complementary sliding mode current control of active power filter. *IEEE Access* **2021**, *9*, 25681–25690. [CrossRef]